Electrospinning Preparation and Luminescence Properties of Europium Complex/Polymer Composite Fibers

Hui Zhang,[†] Hongwei Song,*[,‡] Biao Dong,[‡] Liangliang Han,[†] Guohui Pan,[†] Xue Bai,[‡] Libo Fan,[†] Shaozhe Lu,[†] Haifeng Zhao,[†] and Fang Wang[†]

Key Laboratory of Excited State Physics, Changchun Institute of Optics, Fine Mechanics and Physics, Chinese Academy of Sciences, and Graduate School of Chinese Academy of Sciences, 16 Eastern Nan-Hu Road, Changchun 130033, P. R. China, and State Key Laboratory of Integrated Optoelectronics, College of Electronic Sciences and Engineering, Jilin University, 2699 Qianjin Street, Changchun, 130012, P.R. China

Received: December 6, 2007

The europium complex $Eu(TTA)_3(TPPO)_2$ (TTA = thenoyltrifluoroacetone, TPPO = triphenylphosphine oxide) was incorporated into poly(methyl methacrylate) (PMMA, $M_w \approx 350\,000$), polystyrene (PS, $M_w \approx 250\,000$), poly(vinyl pyrrolidone) (PVP, $M_w \approx 1\,300\,000$) matrixes and electrospun into various composite fibers. The thermal stability of these composite fibers is better than that of the pure europium complex. Their photoluminescence properties were studied in comparison to those of the pure complex. The results indicate that, in all of the composite fibers, the excitation bands of the ligands split into different components because of the distorted crystal field, which reduces the degree to which the $^5D_0-{}^7F_0$ transition is parity-forbidden. In addition, the thermal stability of the photoluminescence of Eu^{3+} in the composite fibers is considerably improved over that of the pure complex. Also, the $Eu(TTA)_3(TPPO)_2$/PS composite fibers exhibit better photostability upon exposure to ultraviolet light. In the $Eu(TTA)_3(TPPO)_2$/PS composite, blue and green band emissions caused by fluorescent impurities appear and, together with the red emissions of Eu^{3+}, produce white light, which might have a potential application in white light-emitting diodes (LEDs).

I. Introduction

Europium complexes have good luminescent properties because of the antenna effect of ligands and the f−f electron transition of Eu^{3+} ions, resulting in important applications in laser, phosphor, and optical data storage devices based on photoluminescent, electroluminescent, and hole-burning spectroscopes. However, pure complexes usually do not have good thermal and mechanical stabilities and processing ability, which restricts the complexes to promising extensive photophysical applications and limited practical uses. To overcome these shortcomings, europium complexes usually must be incorporated into organic, inorganic, or organic/inorganic hybrid matrixes, such as zeolites or mesoporous materials,[1,2] sol−gel silica, or organically modified silicates (ORMOSILs)[3,4] and polymers.[5–11] The polymer-capped rare earth complexes have improved properties, can be processed from solution, and are mechanically flexible.[9] Rare earth complexes incorporated in polymer matrixes embody a new class of materials that present the characteristics of both the complexes and polymers, making them applicable in a wide range of new technologies.

One-dimensional (1D) nanostructures have attracted much attention in recent years because of their importance for both fundamental studies and technological applications.[12] A large number of synthesis and fabrication methods have already been demonstrated for generating 1D nanostructures in the form of fibers, wires, rods, belts, tubes, spirals, and rings from various materials.[13] Among these methods, electrospinning is attracting rapidly increasing attention as a simple electrostatic method for generating 1D nanostructures from organic−inorganic materials.[14–18] In a typical process, a solution is injected from a small nozzle under the influence of an electric field, travels for a certain distance in the air, and is collected as a fiber mat on a grounded collector plate.

Previously, we prepared composite fibers of the europium complex $Eu(TTA)_3(TPPO)_2$ (TTA = thenoyltrifluoroacetone, TPPO = triphenylphosphine oxide) and poly(vinyl pyrrolidone) (PVP, $M_w \approx 1\,300\,000$) by electrospinning, because PVP's good stabilizing and solubilizing capacity and good biological compatibility make it one of the most frequently used specialty polymers.[19] The thermal stability of the photoluminescence of the composite fibers was considerably improved over that of the pure complex; however, the photoluminescence quantum efficiency of Eu^{3+} in the $Eu(TTA)_3(TPPO)_2$/PVP composite fibers was still lower than that of the pure $Eu(TTA)_3(TPPO)_2$ complex. This decrease of the quantum efficiency in the composite fibers might be caused by the influence of hydroxyl groups adsorbed by PVP, which generally act as nonradiative relaxation channels. In this study, we employed poly(methyl methacrylate) (PMMA, $M_w \approx 350\,000$) and polystyrene (PS, $M_w \approx 250\,000$) in addition to PVP as matrixes for the preparation of various $Eu(TTA)_3(TPPO)_2$/polymer composite fibers. One of the objectives was to determine whether a large variety of polymers could be used to stabilize the rare earth complex. PMMA is an amorphous polymer with high optical clarity, which makes it important for applications in which light transmission is necessary. PS is rigid, transparent, and easy to process (shrinkage is low). In addition, PMMA and PS rarely adsorb hydroxyl groups because of their structures. The molecular structures of the PMMA, PS, and PVP polymers and

* Corresponding author. E-mail: hwsong2005@yahoo.com.cn. Fax: 86-431-86176320.
[†] Chinese Academy of Sciences and Graduate School of Chinese Academy of Sciences.
[‡] Jilin University.

10.1021/jp7115005 CCC: $40.75
Published on Web 05/30/2008

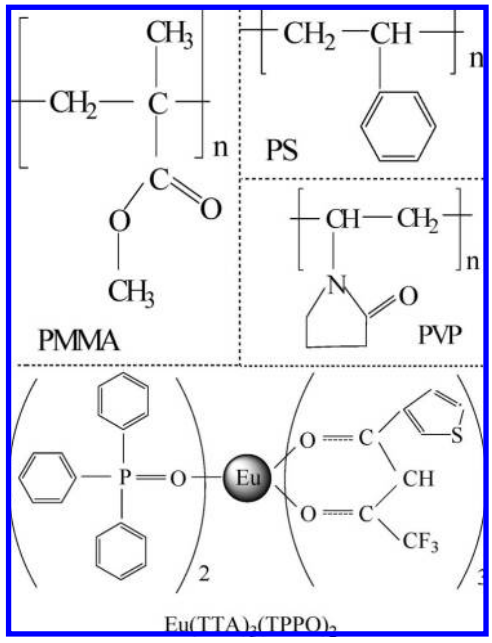

Figure 1. Molecular structures of polymers PMMA, PS, and PVP and of the $Eu(TTA)_3(TPPO)_2$ complex.

the $Eu(TTA)_3(TPPO)_2$ complex are shown in Figure 1. From Figure 1, one can see that PVP has a ketone structure, which can be easily changed to an enol structure under the influence of the nitrogen atom, adsorbing hydroxyl group. PMMA and PS do not have such a problem. It is expected that, in the $Eu(TTA)_3(TPPO)_2$/PMMA and $Eu(TTA)_3(TPPO)_2$/PS composite fibers, the quantum efficiency of Eu^{3+} could be improved over that of the pure $Eu(TTA)_3(TPPO)_2$ complex.

II. Experimental Section

A. Preparation of Precursor Solutions. $Eu(TTA)_3(TPPO)_2$ was synthesized according to the traditional method described in the literature.[20] In the preparation of precursor solutions, ethanol was used as the solvent for the PVP solution because of its high solubility. *N*,*N*-Dimethylformamide (DMF) was used as the solvent for the PMMA and PS solutions because it tends to reduce bead formation and fiber diameters because of its high dielectric constant. The PMMA electrospinning solution was prepared by dissolving 120 mg/mL PMMA in DMF, after which 0.25 wt % $Eu(TTA)_3(TPPO)_2$ relative to PMMA was dissolved in the prepared PMMA solution with stirring. The PS solution was prepared by dissolving 3 g of PS in 10 mL of DMF and then adding 0.25 wt % $Eu(TTA)_3(TPPO)_2$ relative to PS to the prepared PS solution with stirring. To prepare a uniform fiber by electrospinning, 1% tetrabutylammonium chloride (TBAC) relative to PS was added under vigorous stirring. The PVP solution was prepared by dissolving 20 mg of PVP in 10 mL of ethanol. After this solution had been stirred, 0.25 wt % $Eu(TTA)_3(TPPO)_2$ relative to PVP was dissolved in the prepared PVP solution with stirring.

B. Electrospinning Preparation. A schematic diagram of the electrospinning setup is shown in Figure 2a. It consists of three major components: a high-voltage power supply, a spinneret (needle), and a collector plate (grounded conductor). The electrospinning products depend not only on the organic matrix and the concentration, but also on the applied voltage and the distance between the spinneret and the collector plate. In the preparation of $Eu(TTA)_3(TPPO)_2$/PMMA composite fibers, the voltage used was 14 kV, and the distance between

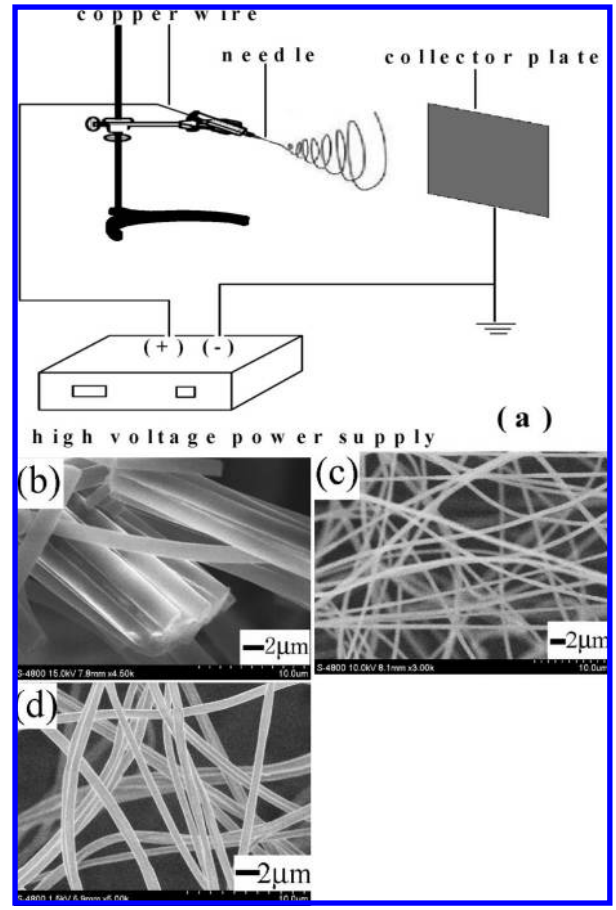

Figure 2. (a) Schematic diagram of the electrospinning setup and SEM images of (b) Eu/PMMA, (c) Eu/PS, and (d) Eu/PVP composite fibers.

the spinneret and collector plate was held at 30 cm. In the preparation of $Eu(TTA)_3(TPPO)_2$/PS fibers, the applied voltage was 18 kV, and the collection distance was 25 cm. In the preparation of $Eu(TTA)_3(TPPO)_2$/PVP fibers, the applied voltage was 13 kV, and the collection distance was 25 cm. In the following text, the pure $Eu(TTA)_3(TPPO)_2$ complex and the $Eu(TTA)_3(TPPO)_2$/PMMA, $Eu(TTA)_3(TPPO)_2$/PS, and $Eu(TTA)_3(TPPO)_2$/PVP composite fibers are denoted Eu complex, Eu/PMMA, Eu/PS, and Eu/PVP, respectively.

C. Measurements. The size and morphology of the composite fibers were obtained using an S-4800 scanning electron microscope (Hitachi). Fourier transform infrared (FTIR) spectra were recorded on a Bio-Rad FTS-3000 (Excalibur Series) spectrometer. Thermogravimetric analysis (TGA) was performed on a Perkin-Elmer Pyris Diamond thermogravimetric analyzer under nitrogen atmosphere at a heating rate of 10 °C/min. The excitation and emission spectra were recorded at room temperature using a Hitachi F-4500 spectrophotometer equipped with a continuous 150-W Xe arc lamp. In the measurements of fluorescence dynamics, 355-nm light from a Nd^{3+}:YAG (yttrium aluminum garnet) laser combined with a third-harmonic generator was used as the pump. An oscilloscope was used to record the decay dynamics. The refractive indexes of TTA and TPPO were measured with a spectroscopic ellipsometer (Jobin Yvon HORIBA). In the measurements of the temperature dependence of the fluorescence, the samples were placed in a liquid-nitrogen cycling system (pellet). A continuous 325-nm beam from a He−Cd laser was used as the excitation source. The fluorescence was measured on a UV-Laboratory Raman Infinity instrument (Jobin Yvon Company) with a resolution of 2 cm^{-1}. In the

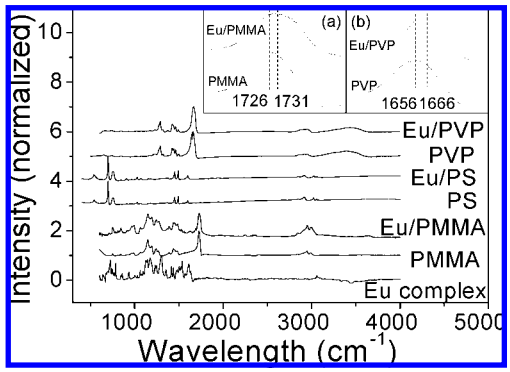

Figure 3. FTIR spectra of the Eu complex; pure PMMA, PS, and PVP fibers; and Eu/PMMA, Eu/PS, and Eu/PVP composite fibers.

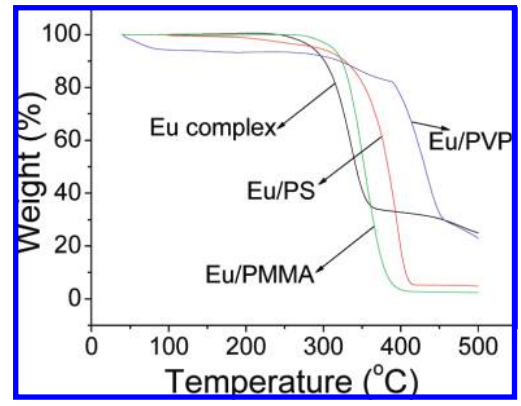

Figure 4. TGA traces obtained at 10 °C/min under flowing N_2.

experiments of spectral change induced by ultraviolet (UV) irradiation, monochromic light separated from the continuous 150-W Xe arc lamp was used as the irradiation source, with a slit of 10 nm.

III. Results and Discussion

A. Characterization of Structure and Morphology. Figure 2b−d shows scanning electron microscope (SEM) images of composite fiber samples Eu/PMMA, Eu/PS, and Eu/PVP, respectively. From these images, one can see that uniform fibers formed in all of the composite samples. The average diameters for the Eu/PMMA, Eu/PS, and Eu/PVP composites were ∼1400, 800, and 700 nm, respectively. Note that the morphology of the electrospinning composites depends strongly on the concentration of the organic polymers in the preparation. For the Eu/PMMA composites, when the concentration of PMMA was low (<80 mg/mL), some beads formed. When the concentration of PMMA was too high, electrospinning products were rarely obtained. In fact, the polymer concentration is a key factor influencing the viscosity of the polymer solution, which plays an important role in the process of electrospinning. In this work, the concentration of PMMA in the Eu/PMMA sample was 120 mg/mL. In the preparation of Eu/PS composites, some beads were easily formed, but when TBAC was added at a certain concentration (1% relative to PS), the beads disappeared. The addition of a soluble organic salt (TBAC) to the PS solution increases the conductivity of the solution.[21]

Figure 3 shows the FTIR spectra of different samples. The FTIR spectra of these composite fibers are similar to those of the corresponding polymer fibers in the studied range. For the PMMA fibers and sample Eu/PMMA, the absorption bands in the range of 2900−3000 cm^{-1} correspond to C−H vibrations. The band at 1726 cm^{-1} for the PMMA fibers corresponds to the C═O vibration, whereas for the Eu/PMMA fibers, it shifts to 1731 cm^{-1} (see the inset of Figure 3a). This indicates that the Eu complex is stabilized through chemical interactions with the oxygen atoms of the carbonyl group of PMMA. This interaction might come from the donation of a pair of electrons from the carbonyl oxygen to the lanthanide ions. For the PS fibers and sample Eu/PS, the absorption bands at 697, 756, 1028, 1450, 1492, and 1600 cm^{-1} are assigned to the vibrations of the benzenoid ring. These bands maintain the same positions for the PS and Eu/PS fibers, which suggests that the Eu complex has little chemical interaction with PS, but physically mixes with it uniformly. For the PVP fibers, the peak at 1656 cm^{-1} is assigned to the C═O stretching band, which is the typical mode of PVP. In the Eu/PVP fibers, this band shifts to 1666 cm^{-1} (see the inset of Figure 3b), which suggests that the Eu complex is stabilized through chemical interactions with the oxygen atoms of the carbonyl group of PVP, as in sample Eu/PMMA. The $Eu(TTA)_3(TPPO)_2$ complex used to fabricate the composite fibers is a nonhydrated complex, which can be verified by the absence of the O−H stretching mode in the IR absorption spectrum for the pure Eu complex. A broad band at 3400 cm^{-1} appears in the spectra of the Eu/PVP and PVP fibers, which is generated by the vibrations of the associated hydroxyl groups. The contamination of trace hydroxyl groups in Eu/PVP and PVP fibers occurred in the electrospinning solution.

B. Thermal Properties. To determine the thermal stability of the composite fiber samples, TGA experiments were performed; the results are displayed in Figure 4. The weight decrease below 100 °C (5 wt %) for Eu/PVP is assigned to loss of residual ethanol. The weight loss of Eu/PS below 280 °C (∼5 wt %) is attributed to the loss of the dopant TBAC and residual solvent.[22] The decomposition temperatures (T_d) of the Eu complex, Eu/PMMA, and Eu/PS are about 335 °C (66 wt %), 354 °C (96 wt %), and 394 °C (90 wt %), respectively. For Eu/PVP, there are two decomposition points in the studied range: the T_d values are about 342 °C (12 wt %) and 431 °C (50 wt %).[23] It can be seen that the thermal stabilities of Eu/PS, Eu/PMMA, and Eu/PVP are better than that of the Eu complex. For Eu/PMMA and Eu/PVP, the better thermal stability can be attributed to the chemical bonding of the Eu complex with the oxygen atoms of the carbonyl groups in PMMA and PVP, which results in the the decomposition of the Eu complex together with PMMA and PVP. For Eu/PS, the rigid PS matrix makes the Eu complex more stable.

C. Excitation and Emission Spectra of Eu^{3+}. The photoluminescence properties of the composite fibers were studied and compared with those of the pure europium complex. Figure 5 shows the excitation and emission spectra of various samples. In the pure complex, a broad excitation band extending from 200 to 400 nm appears, which is assigned to the $\pi-\pi^*$ electron transition of the ligands. In the composites, it is interesting to observe that the excitation bands split into several components, having peaks at ∼210, ∼266, and ∼347 nm in Eu/PMMA; at ∼278, ∼280, and ∼351 nm in Eu/PS; and at ∼233, ∼262, ∼287, ∼344, and ∼372 nm in Eu/PVP. This indicates that, in the composites, because of the presence of the surrounding polymer medium, the site symmetry decreases.[24] In addition, in the excitation spectrum of the pure complex, the $^7F_0-^5D_2$ inner-shell excitation line appears, whereas in the composites, this line disappears. This suggests that, in the composites, the f−f inner-shell transitions are completely quenched through nonradiative energy transfer from the higher excited states to the organics or some unidentified defect levels, substituting for nonradiative relaxation from higher excited states to $^5D_0$.

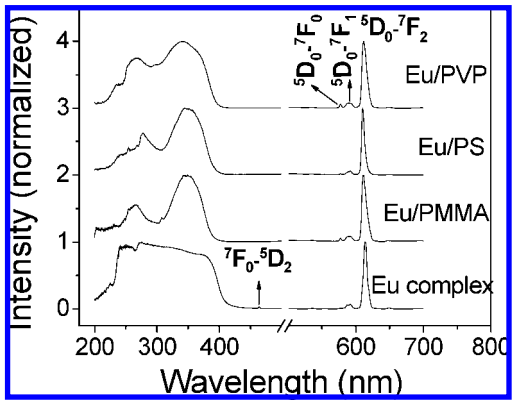

Figure 5. Excitation spectra ($\lambda_{em} = 611$ nm) and emission spectra ($\lambda_{ex} = 340$ nm) for the $^5D_0-^7F_J$ transitions of Eu^{3+} in different samples.

In the emission spectra, the red $^5D_0-^7F_J$ ($J = 0-2$) transitions of Eu^{3+} ions are clearly observed. In the pure complex, only the $^5D_0-^7F_1$ and $^5D_0-^7F_2$ lines appear, whereas the $^5D_0-^7F_0$ emission is completely absent. In the composite fibers, the $^5D_0-^7F_0$ emissions can be identified. This indicates that the electric-dipole $^5D_0-^7F_0$ emissions become partly allowed because of the distorted crystal field, whereas it is completely forbidden in the pure complex. The emission spectra also show that the main line of the $^5D_0-^7F_2$ transition for Eu^{3+} in the composites blue shifts in contrast to that in the pure europium complex. The reason for this shift is that the relative contributions of different Stark components of the $^5D_0-^7F_2$ transition are different in different samples, which can be further verified by high-resolution emission spectra. In contrast to the pure complex, the emission lines in the composite fibers become broader to different degrees, which can be attributed to heterogeneous broadening caused by more disordered local environments surrounding the Eu^{3+} ions.

It is well-known that the magnetic-dipole transitions $^5D_0-^7F_1$ are nearly independent of the ligand field and therefore can be used as an internal standard to account for ligand differences.[25] The electric-dipole transitions $^5D_0-^7F_2$, the so-called hypersensitive transitions, are sensitive to the symmetry of the coordination sphere. The intensity ratio of the magnetic-dipole transition to the electric-dipole transition in the lanthanide complex measures the symmetry of the coordination sphere.[26] The intensity ratios of the $^5D_0-^7F_2$ transition to the $^5D_0-^7F_1$ transition in the pure Eu complex and the Eu/PMMA, Eu/PS, and Eu/PVP composites were determined to be 11.5, 13.0, 13.8, and 10.2, respectively. These results suggest that, when the Eu complex is incorporated into the microcavities of the polymer matrix, the Eu^{3+} ions exhibit different local environments because of the influence of the surrounding polymer. The symmetry of the coordination sphere for the Eu^{3+} ions increases slightly in the Eu/PMMA and Eu/PS composites but decreases slightly in the Eu/PVP composite.

To study the local environments surrounding Eu^{3+} further, high-resolution emission spectra and decomposed spectra of the $^5D_0-^7F_2$ transitions for the Eu^{3+} ions in the various samples at 10 K are presented in Figure 6, which also shows some distinctive differences between the pure complex and the composite fibers. In the pure Eu complex, five crystal-field splitting lines of the $^5D_0-^7F_2$ transition can be observed at 611.3, 614.4, 616.6, 618.8, and 621.1 nm. The line at 616.6 nm is the strongest. In the composite fibers, because of more disordered local environments surrounding Eu^{3+} caused by the influence of the polymers, the sublines of the $^5D_0-^7F_2$ transition are broadened inhomogeneously and overlap each other, forming a broad line. The intensity maxima in Eu/PMMA, Eu/PS, and Eu/PVP are located at 613.2, 612.3, and 614.3 nm, respectively. From the decomposed spectra, it can be seen that, in addition to the spectral broadening and shift, the relative intensities of different Stark components in the composites also vary greatly in comparison to those in the pure complex.

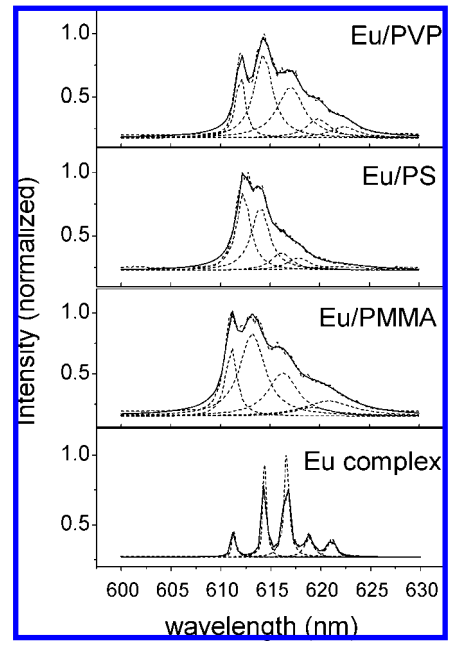

Figure 6. High-resolution emission spectra of the Eu complex, Eu/PMMA, Eu/PS, and Eu/PVP and five Lorentzian fitting functions.

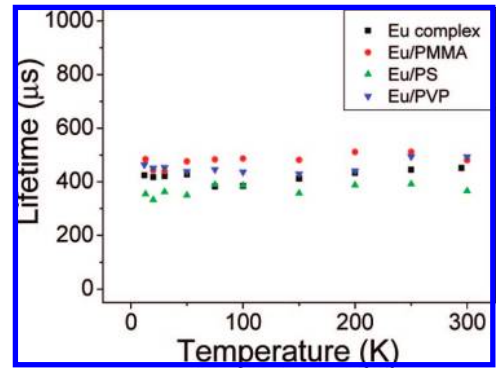

Figure 7. Dependence of the exponential decay time constant of the $^5D_0-^7F_2$ transition ($\lambda_{em} = 614$ nm) on temperature for various samples.

D. Fluorescence Dynamics of Eu^{3+} Ions. To determine the radiative and nonradiative transition processes in the various composite fibers, the luminescent decay dynamics of the $^5D_0-^7F_2$ emissions for Eu^{3+} ions under 355-nm excitation were measured at different temperatures. The results indicate that the $^5D_0-^7F_2$ emissions decay exponentially in all of the samples. The dependence of the exponential decay time constant of the $^5D_0-^7F_2$ transition on temperature in various samples is shown in Figure 7. This figure reveals the following two observations: (1) In the range of 10−300 K, the decay time constant of the $^5D_0-^7F_2$ transition remains nearly constant for all of the samples. (2) In the Eu complex and the different composite fibers, the decay time constant of the $^5D_0-^7F_2$ transition does not change greatly. As is well-known, the luminescent decay time constant is the inverse of the sum of the radiative and nonradiative transition rates. The radiative transition rate is nearly indepen-

TABLE 1: Variation of the $^5D_0-^7F_2$ Decay Time Constants (μs) Measured at Different Wavelengths at 10 K

sample	612 nm	614 nm	616 nm	618 nm	621 nm
Eu complex	307.7 ± 1.4	472.9 ± 0.6	507.6 ± 0.3	527.3 ± 0.2	484.7 ± 0.5
Eu/PMMA	530.8 ± 0.3	537.2 ± 0.2	538.8 ± 0.3	546.3 ± 0.3	516.2 ± 0.3
Eu/PS	446.8 ± 0.4	471.4 ± 0.3	448.0 ± 0.3	461.3 ± 0.4	461.1 ± 0.4
Eu/PVP	466.9 ± 0.7	464.0 ± 0.6	456.8 ± 0.7	506.3 ± 0.6	440.5 ± 0.8

dent of temperature, whereas the nonradiative relaxation rate decreases strongly with temperature. The above results imply that the nonradiative relaxation can be neglected below room temperature and that the decay time constant is dominated by the radiative transition rate,[27] which can be written as

$$\tau_R \approx \frac{1}{f(\mathrm{ED})} \frac{{\lambda_0}^2}{\left[\frac{1}{3}(n^2+2)\right]^2 n} \quad (1)$$

where f(ED) is the oscillator strength for the electric-dipole transition, λ_0 is the wavelength in a vacuum, and n is the refractive index of the material. Meltzer et al. observed that the radiative lifetime of nanocrystals depends not only on the refractive index itself, but also on the surrounding medium and deduced that, for nanoparticles, n in eq 1 should be substituted by the effective index $n_{\mathrm{eff}} = xn + (1 - x)n_{\mathrm{med}}$, where x is the filling factor describing the fraction of the space occupied by the nanoparticles and n_{med} is the refractive index of the surrounding medium.[28] For the present composite fibers, the radiative lifetime should depends on not only the Eu complex, but also on the surrounding polymer. The refractive indexes of the various components are 1.56 for TTA, 1.72 for TPPO, 1.53 for PVP,[29] 1.45 for PMMA, and 1.59 for PS.[30] The refractive indexes of the Eu complex and the fibers containing the different polymers exhibit only a slight change; therefore, the surrounding media (PMMA, PS, and PVP) should have little influence on the radiative lifetime of europium.

Table 1 lists the decay time constants of the $^5D_0-^7F_2$ transition measured at different wavelengths corresponding to different Stark components in the various samples. From Table 1, one can see that, in the pure complex, the decay time constants corresponding to the different Stark components vary greatly. In contrast, the values are essentially identical in all of the composite fibers. The reason for this difference should be that, in the composite fibers, different Stark components overlap each other owing to the more disordered local environments surrounding Eu^{3+}. The refractive index should be the same for each component in one Eu complex, so the change in decay time constant with Stark component should be related to the variation of the oscillator strength. The oscillator strength of the Eu complex also changes when the complex is incorporated into the polymer matrixes. The change of radiative decay time depends on both the change of the crystal field and the refractive index of the surrounding polymer matrix.

E. Temperature Dependence of the Eu^{3+} Emissions. The emission spectra of Eu^{3+} in various samples were measured at different temperatures under 325-nm excitation. Figure 8a,b shows the $^5D_0-^7F_2$ emission spectra of Eu^{3+} ions measured at 81 and 321 K in the Eu complex and the Eu/PS composite fibers, respectively. For both the pure complex and the composite fibers, the spectra reveal that (1) the full width at half-maximum (fwhm) becomes broader with increasing temperature, (2) the locations of all of the Stark peaks shift slightly to shorter wavelengths, and (3) the relative strengths of different Stark components change with temperature. The intensities of the Stark peaks at longer wavelengths increase relative to those of the peaks at shorter wavelength. For the other two composites, the results are similar. The increased line width can be attributed to the more disordered local environments surrounding the Eu^{3+} ions induced by increased thermal vibration of the lattices. The increased temperature will also lead to the expansion of the lattices; as a consequence, the influence of the crystal field on the energy level of Eu^{3+} decreases, and the emission lines blue shift.

Figure 9 shows the emission intensity of the $^5D_0-^7F_2$ transition for Eu^{3+} as a function of temperature. It is obvious that the variation of the emission intensity for the Eu^{3+} ions in the composite fibers is markedly different from that in the pure complex. The emission intensity of the pure $Eu(TTA)_3(TPPO)_2$ complex powder decreases monotonically with increasing

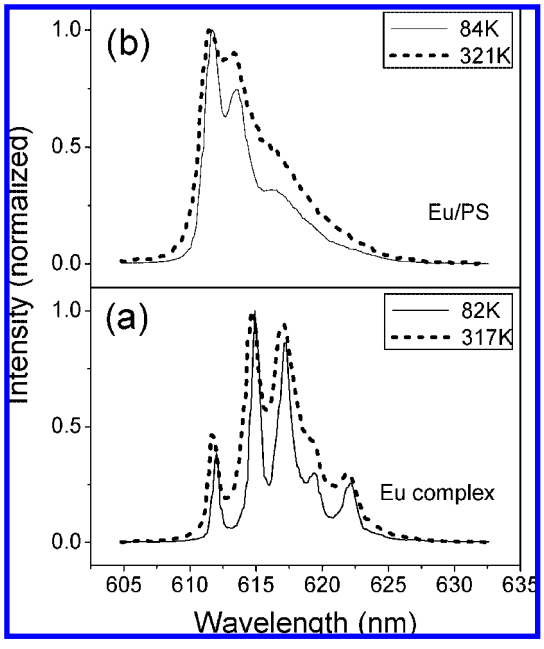

Figure 8. $^5D_0-^7F_2$ emission spectra of Eu^{3+} ions excited by a 325-nm laser measured at 81 and 321 K in (a) the Eu complex and (b) the Eu/PS composite.

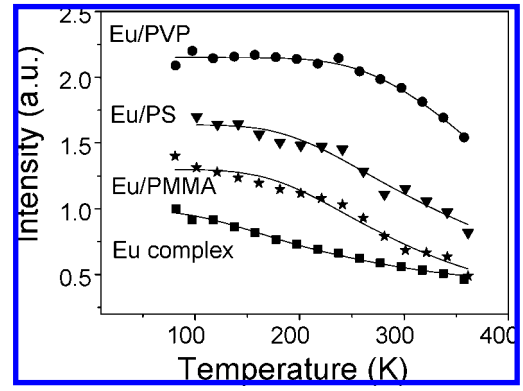

Figure 9. Dependence of the emission intensity of the $\Sigma^5D_0-^7F_J$ transitions on temperature for various samples.

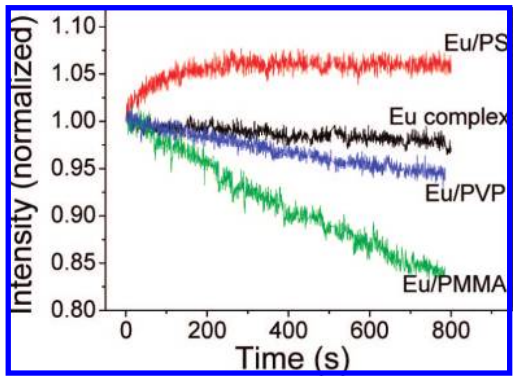

Figure 10. Dependence of the normalized intensity at 611 nm on irradiation time for different samples. The samples were irradiated with 350-nm light.

temperature in the studied range. For the composite fibers, the total emission intensity of the Eu^{3+} ions changes little at low temperature and then decreases quickly as the temperature increases continuously. In Figure 8, the intensity as a function of temperature can be well fitted by the well-known thermal activation function[31]

$$I(T) = \frac{I_0}{1 + \alpha e^{-E_A/k_B T}} \quad (2)$$

where I_0 is the emission intensity at 0 K, α is a proportionality coefficient, E_A is the thermal activation energy, k_B is the Boltzmann constant, and T is the absolute temperature. The values of E_A for the Eu complex and the Eu/PMMA, Eu/PS, and Eu/PVP composites were determined to be 40.3, 126.7, 120.8, and 201.4 meV, respectively. The improved values of E_A for the composite fibers suggest that the thermal stabilities of the photoluminescence are much better than that in the pure complex. It is suggested that, in the composites, because of the presence of the polymer matrixes, the vibrational transitions of the complexes are constrained, leading to the improvement in the thermal stability of the photoluminescence.[9] The polarities and concentrations of the polymers will also influence the stability of the composite fibers.

F. Photoluminescence Stability. To compare the photoluminescence stability, UV-induced spectral changes in the different samples were also studied. Figure 10 shows the dependence of the normalized emission intensity of the $^5D_0-^7F_2$ transition (611 nm) on irradiation time for the different samples. It can be seen that the emission intensity of the $^5D_0-^7F_2$ transition in the pure Eu complex decreases with increasing exposure time; the emission intensities of Eu/PMMA and Eu/PVP exhibit larger decreases than that of the Eu complex. The same decrease was also found for $Eu(BA)_3(TPPO)_2$/PVP composite fibers, which can be improved by increasing the concentration of PVP.[32] The photoluminescence stabilities of Eu/PMMA and Eu/PVP could possibly be improved by increasing the concentrations of these polymers as well. It is interesting to observe that the intensity of Eu/PS actually increases with increasing exposure time. In fact, the PS polymer provides a rigid environment for the pure complex to reduce the energy consumption of vibrations of ligands and intermolecular collisions of complexes. The rigid PS molecule protects the pure complexes from decomposing under UV irradiation. The intensity enhancement with exposure time in Eu/PS can be attributed to optical modification of the surface defects. In the preparation of this material, some surface defects are involved between the pure complex and PS, which generally act as

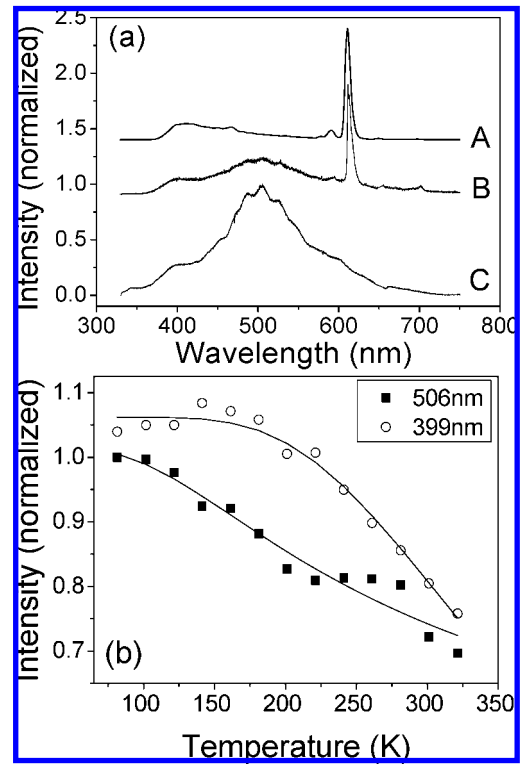

Figure 11. (a) Emission spectra of Eu/PS excited by 325-nm light from (A) a continuous 150-W Xe arc lamp and (B) a He−Cd laser and (C) the spectrum of pure PS under 325-nm laser excitation. (b) Temperature dependence of the fluorescence intensity of PS measured under 325-nm excitation in Eu/PS composite fiber.

nonradiative relaxation channels. Under UV exposure, the defects are gradually modified, causing the photoluminescence to increase.[33]

G. Photoluminescence Spectra of PS. It is interesting to point out that, in addition to the red emissions of Eu^{3+}, band emissions in the blue and green ranges were also observed for the Eu/PS composite fibers. Figure 11a shows the emission spectra of the Eu/PS composite fibers in contrast to those of pure PS fibers under 325-nm excitation at room temperature. Under 325-nm laser excitation, a broad band peaking around 505 nm appears for both the pure PS fibers and the Eu/PS composite fibers. The band consists of different components, including a shoulder appearing around 403 nm. In comparison, one can conclude that the band emission is caused by the PS host. It is believed that the blue emission at about 403 nm is caused by strongly fluorescent impurities in PS, present at low concentration and forming part of the macromolecules.[34] Fluorescence in the blue region might be due to chromophores formed by conjugated double bonds and phenyl groups.[34] In fact, such chromophores have been found to be present in all commercial samples at smaller concentrations or in the laboratory. Rather extended conjugated π-electron systems or large Stokes shifts might account for the long-wavelength fluorescence band peaking around 505 nm. Fluorescence emissions near 400 nm and strong Stokes shifts have been reported for *cis*-stilbene and similar compounds as solids and in solid solutions.[35] Furthermore, some studies of the spectroscopy of various polymers based on stilbene units have reported both broad structureless red-shifted emission[36] and red-shifted structured fluorescence.[37] The band emission under the excitation of a 325-nm Xe lamp is considerably different from that observed under the excitation of a 325-nm laser. The emission peak around 403 nm increases greatly relative to the peak around 505 nm and

becomes the emission maximum. The most obvious difference between the laser and lamp sources is that the former is a polarized beam and the latter is not. It is suggested that the band emissions caused by fluorescence impurities are dependent on the polarization direction of the incident beam.

The peaks at 505 and 403 nm also show different temperature-dependent behaviors. Figure 11b shows the temperature dependence of emission intensity for the two emission bands caused by PS under 325-nm excitation for the Eu/PS composite. It can be seen that the peak at 505 nm simply decreases continually with increasing temperature. The peak at 403 nm remains nearly constant below 200 K and decreases rapidly above 200 K. The intensity as a function of temperature can also be well fitted by eq 2. The values of E_A were deduced to be 34.9 and 108.6 meV, respectively, for the peaks at 506 and 403 nm, implying that the thermal stability of the emission at 403 nm is better than that of the 505-nm emission.

It should be mentioned that, for the Eu/PS composite, the red emission caused by Eu^{3+} and the green and blue emissions caused by PS can form white light if the content of the Eu complex is controlled or the temperature is adjusted. Because the excitation wavelength can be tuned from 200 to 400 nm in the Eu/PS composite, it is suitable for use as a potential white light material in light-emitting diodes (LEDs) under the excitation of ultraviolet light.

H. Luminescent Quantum Efficiency. The luminescent quantum efficiencies under the 325-nm excitation were determined by the integrating sphere method to be 67.1%, 3.2%, 4.1%, and 3.6%, respectively, for the pure complex and the Eu/PMMA, Eu/PS, and Eu/PVP composite fibers. It is obvious that the quantum efficiencies of the present composites are significantly lower than that of the Eu complex. Previously, we prepared the Eu/PVP composite by the same technique, and its quantum efficiency was deduced to be 49.2%, which was only slightly smaller than the quantum efficiency of the pure complex. The mass ratio of the $Eu(TTA)_3(TPPO)_2$ complex to PVP was 2.5 wt %.[19] The mass ratio of the $Eu(TTA)_3(TPPO)_2$ complex to PVP in the present Eu/PVP composite fiber is only 0.25 wt %. These results indicate that the luminescent quantum efficiency of the composite fibers depends strongly on the ratio of the Eu complex to the polymer. An increase in the content of the Eu complex leads to an increase of the luminescent quantum efficiency. A reason for this trend is that, in the composite fibers, the polymers also adsorb the excitation light. This part of energy cannot be transferred to the Eu complex, leading to energy loss. The lower the content of polymer, the lower the energy loss. Therefore, the ratio of the Eu complex to the polymer is a key factor influencing the luminescent quantum efficiency of the composite fibers. Unexpectedly, for the present composite fibers, the luminescent quantum efficiency varies only slightly, suggesting that the contamination of hydroxyl groups in PVP is not a main factor influencing the luminescent quantum efficiency as the content of the Eu complex is small. The small increase of luminescent quantum efficiency in the Eu/PS composite in contrast to the Eu/PMMA and Eu/PVP composites can be attributed to the contribution of the photoluminescence of PS.

IV. Conclusions

In summary, uniform $Eu(TTA)_3(TPPO)_2$/PMMA, $Eu(TTA)_3(TPPO)_2$/PS, and $Eu(TTA)_3(TPPO)_2$/PVP composite fibers were prepared by electrospinning, and their photoluminescence properties were studied in comparison to those of the pure complex. The results demonstrate that, because of the distortion of the crystal field, the excitation bands of the $\pi-\pi^*$ electron transition of the ligands split into different components. The luminescent decay time constants for the $^5D_0-^7F_2$ transitions in the composite fibers vary only slightly from those of the pure complex, depending on the refractive index of the surrounding polymer matrix and the crystal field. Most importantly, for the composite fibers, the thermal stability and the temperature stability of the photoluminescence are much better than those of the pure complex because of the modification of the polymer matrixes. The photostability of the luminescence for Eu/PS improved considerably in comparison to that for the Eu complex. In addition, it is interesting to observe that the emission intensity increased with increasing irradiation time. The photoluminescence quantum efficiency of the composites depends mainly on the mass ratio of the Eu complex to the polymer. Increased content of the Eu complex leads to an improvement in th quantum efficiency. For the Eu/PS composite fibers, in addition to the red emission of Eu^{3+}, the band emissions of PS can be also observed in the blue and green ranges. This combination can form white light emission under excitation of a ultraviolet LED. Considering the various properties of the composites, PS is a better polymer matrix than the other two polymers. In short, we believe that these novel luminescent composite fibers might have potential applications in a wide range of new technologies.

Acknowledgment. The authors gratefully acknowledge the financial support of the Nation Natural Science Foundation of China (Grants 10704073, 50772042, and 10504030) and the 863 National Key Project of China (2007AA03Z314).

References and Notes

(1) Alvaro, M.; Fornes, V.; Garsia, S.; Garasia, H.; Scaiano, J. C. *J. Phys. Chem. B* **1998**, *102*, 8744.
(2) Xu, Q.; Li, L.; Liu, X.; Xu, R. *Chem. Mater.* **2002**, *14*, 549.
(3) Li, H.; Inouem, S.; Machida, K.-I.; Adachi, G.-Y. *Chem. Mater.* **1999**, *11*, 3171.
(4) Strek, W.; Sokolnicki, J.; Legendziewicz, J.; Maruszewski, K.; Reisfeld, R.; Pavich, T. *Opt. Mater.* **1999**, *13*, 41.
(5) Feng, H.-Y.; Jian, S.-H.; Wang, Y.-P.; Lei, Z.-Q.; Wang, R.-M. *J. Appl. Polym. Sci.* **1998**, *68*, 1605.
(6) Ling, Q.; Yang, M.; Wu, Z.; Zhang, X.; Wang, L.; Zhang, W. *Polymer* **2001**, *42*, 4605.
(7) Wang, L.-H.; Wang, W.; Zhang, W.-G.; Kang, E.-T.; Huang, W. *Chem. Mater.* **2000**, *12*, 2212.
(8) Bermudez, V. de Zea; Carlos, L. D.; Silva, M. M.; Smith, M. J. *J. Chem. Phys.* **2000**, *112*, 3293.
(9) Li, Q.; Li, T.; Wu, J. *J. Phys. Chem. B* **2001**, *105*, 12293.
(10) Yang, C. Y.; Srdanov, V.; Robinson, M. R.; Bazan, G. C.; Heeger, A. J. *Adv. Mater.* **2002**, *14*, 980.
(11) Parra, D. F.; Brito, H. F.; Matos, J. D. R.; Dias, L. C. *J. Appl. Polym. Sci.* **2002**, *83*, 2761.
(12) For a review, see: Xia, Y.; Yang, P.; Sum, Y.; Wu, Y.; Mayers, B.; Gates, B.; Yin, Y.; Kim, F.; Yan, H. *Adv. Mater.* **2003**, *15*, 353.
(13) See the special issue: *Adv. Mater.* **2003**, *15*, 351.
(14) Ding, B.; Kim, H.; Kim, C.; Khil, M.; Park, S. *Nanotechnology* **2003**, *14*, 532.
(15) Sui, X. M.; Shao, C. L.; Liu, Y. C. *Appl. Phys. Lett.* **2005**, *87*, 113115.
(16) Rencker, D. H.; Chun, I. *Nanotechnology* **1996**, *7*, 216.
(17) Huang, Z. M.; Zhang, Y. Z.; Kotaki, M.; Ramakrishna, S. *Compos. Sci. Technol.* **2003**, *63*, 2223.
(18) Li, D.; Xia, Y. *Adv. Mater.* **2004**, *16*, 1151.
(19) Zhang, H.; Song, H. W.; Yu, H. Q.; Li, S. W.; Bai, X.; Pan, G. H.; Dai, Q. L.; Wang, T.; Li, W. L.; Lu, S. Z.; Ren, X. G.; Zhao, H. F.; Kong, X. G. *Appl. Phys. Lett.* **2007**, *90*, 103103.
(20) Melby, L. R.; Rose, N. J.; Abramson, E.; Caris, J. C. *J. Am. Chem. Soc.* **1964**, *86*, 5117.
(21) Dong, H.; Nyame, V.; Macdiarmid, A. G.; Jones, W. E., Jr. *J. Polym. Sci. B* **2004**, *42*, 3934.

(22) Dong, H.; Prasad, S.; Nyame, V.; Jones, W. E., Jr. *Chem. Mater.* **2004**, *16*, 371.

(23) Sukpirom, N.; Lerner, M. M. *Chem. Mater.* **2001**, *13*, 2179.

(24) Chang, N. C.; Gruber, J. B. *J. Chem. Phys.* **1964**, *41*, 3227.

(25) Bunzli, J.-C. G. Luminescent Probes. In *Lanthanide Probes in Life, Chemical and Earth Sciences, Theory and Practice*; Bunzli, J.-C. G., Choppin, G. R., Eds.; Elsevier: New York, 1989; p 219.

(26) Kirby, A. F.; Foster, D.; Richardson, F. S. *Chem. Phys. Lett.* **1983**, *95*, 507.

(27) Peng, H. S.; Song, H. W.; Chen, B. J.; Wang, J. W.; Lu, S. Z.; Kong, X. G.; Zhang, J. H. *J. Chem. Phys.* **2003**, *118*, 3277.

(28) Meltzer, R. S.; Feofilov, S.; Tissue, B. M. *Phys. Rev. B* **1999**, *60*, R14012.

(29) Belleville, P.; Bonnin, C.; Lavastre, E.; Pegon, P.; Rorato, Y. *Proc. SPIE* **2001**, *4347*, 588.

(30) Zhao, D.; Qin, W. P.; Zhang, J. S.; Wu, C. F.; Qin, G. S.; De, G. Zhang, J. S.; Lu, S. Z. *Chem. Phys. Lett.* **2005**, *403*, 129.

(31) Li, B. S.; Liu, Y. C.; Zhi, Z. Z.; Shen, D. Z.; Lu, Y. M.; Zhang, J. Y.; Fan, X. W. *J. Cryst. Growth* **2002**, *240*, 479.

(32) Zhang, H.; Song, H.; Yu, H.; Bai, X.; Li, S.; Pan, G.; Dai, Q.; Wang, T.; Li, W.; Lu, S.; Ren, X.; Zhao, H. *J. Phys. Chem. C* **2007**, *111*, 6524.

(33) Xu, Q. H.; Li, L. S.; Liu, X. S.; Xu, R. R. *Chem. Mater.* **2002**, *14*, 549.

(34) (a) Klöpffer, W. *Eur. Polym. J.* **1975**, *11*, 203. (b) Yu, S.-H.; Yoshimura, M.; Moreno, J. M. C.; Fujiwara, T.; Fujino, T.; Teranishi, R. *Langmuir* **2001**, *17*, 1700.

(35) Fischer, G.; Fischer, E.; Stegemeyer, H. *Ber. Bunsen-Ges. Phys. Chem.* **1973**, *77*, 685.

(36) (a) Catal; án, J.; Zimányi, L.; Saltiel, J *J. Am. Chem. Soc.* **2000**, *122*, 2377. (b) Brocklehurst, B.; Bull, D.; Evans, M.; Scott, P.; Stanney, G. *J. Am. Chem. Soc.* **1975**, *97*, 2977. (c) Anger, I.; Sandros, K.; Sundahl, M.; Wennestrom, O. *J. Phys. Chem.* **1993**, *97*, 1929. (d) Letsinger, R. L.; Wu, T. *J. Am. Chem. Soc.* **1994**, *116*, 811.

(37) (a) Oldham, W. J., Jr.; Miao, Y.-J.; Lachicotte, R. J.; Bazan, G. C. *J. Am. Chem. Soc.* **1998**, *120*, 419. (b) Song, X.; Geiger, C.; Furman, I.; Whitten, D. G. *J. Am. Chem. Soc.* **1994**, *116*, 4103. (c) Banan, G. C.; Oldham, W. J., Jr.; Lachicotte, R. J.; Tretiak, S.; Chemyak, V.; Mukamel, S. *J. Am. Chem. Soc.* **1994**, *116*, 811.

JP7115005